Journal of Applied Physics

Conduction mechanism of resistive switching films in MgO memory devices

Cite as: J. Appl. Phys. **111**, 094104 (2012); https://doi.org/10.1063/1.4712628
Submitted: 10 January 2012 • Accepted: 11 April 2012 • Published Online: 10 May 2012

Fu-Chien Chiu, Wen-Chieh Shih and Jun-Jea Feng

Conduction mechanism of resistive switching films in MgO memory devices

Fu-Chien Chiu,[1,a)] Wen-Chieh Shih,[2] and Jun-Jea Feng[1]
[1]*Department of Electronic Engineering, Ming-Chuan University, Taoyuan 333, Taiwan*
[2]*Institute of Electronics Engineering, National Tsing-Hua University, Hsinchu 300, Taiwan*

(Received 10 January 2012; accepted 11 April 2012; published online 10 May 2012)

In this work, nonpolar resistance switching behavior was demonstrated in Pt/MgO/Pt structure. The resistance ratio of high resistance state (HRS) and low resistance state (LRS) is about on the order of 10^5 for the compliance current (I_{comp}) of 1 mA at 300 K. Using enough I_{comp} ($\geq$0.5 mA) during SET processes, the LRS resistances reach a minimum of about 10^2–10^3 Ω and the RESET currents reach a maximum of about 10^{-4}–10^{-3} A. Experimental results indicate that the conduction mechanism in MgO films is dominated by the hopping conduction and the Ohmic conduction in HRS and LRS, respectively. Therefore, the electrical parameters of trap energy level, trap spacing, Fermi level, electron mobility, and effective density of states in conduction band in MgO films were obtained. © *2012 American Institute of Physics*. [http://dx.doi.org/10.1063/1.4712628]

I. INTRODUCTION

Because traditional Flash memory devices are approaching physical limitations, the developments of next generation nonvolatile memory (NVM) devices are in urgent need. Recently, resistance random access memory (RRAM) devices, one of the novel memory devices, have been a promising alternative for the next generation NVM applications.[1] The most attraction of RRAM technology is its good compatibility with the complimentary metal-oxide-semiconductor (CMOS) process,[2] which indicates that the scaling merit will work in terms of the low power consumption of the RRAM operation and then will bring a strong cost-competitiveness to RRAM. Additionally, the merits of RRAM include high switching speed, high durability, small cell size, simple cell structure, and multi-state switching.[1–4] There are several types of materials used in RRAM, such as perovskite-type oxides,[1,3,5] binary metal oxides,[2–4,6] organic compounds,[7,8] amorphous Si,[9] and solid-state electrolytes.[4] Among the RRAM materials being studied, binary metal oxides are most favorable because of their simple constituents, compatible with CMOS processes, and resistive to thermal/chemical damages.[2,4,6,10]

Magnesium oxide (MgO) is a chemically inert material which has a large band gap (7–8 eV), a high dielectric constant (6–10), a high thermal conductivity, and a high breakdown field (~12 MV/cm).[11] Therefore, MgO thin films may have the potential to ensure adequate band offsets and to reduce leakage currents in device applications. Recently, MgO thin films were used to study the applications of RRAM devices.[11–15] Although the resistance switching characteristics and thin film reliability were studied, the current conduction mechanisms in MgO films have not been addressed in detail. In this work, MgO thin films were deposited by radio frequency (*rf*) magnetron sputtering. The behavior of nonpolar resistance switching in Pt/MgO/Pt metal-insulator-metal (MIM) structure was demonstrated. The high resistance state (HRS)/low resistance state (LRS) resistance ratio is about on the order of 10^5 at room temperature and increases with increasing temperature. Experimental results show that the dominant conduction mechanism in MgO films is the hopping conduction and the Ohmic conduction in HRS and LRS, respectively. At room temperature the trap energy level, the trap spacing, and the effective density of states in conduction band in MgO films were determined to be about 0.7 eV, 1.0 nm, and 1.9×10^{15} cm^{-3}, respectively.

II. EXPERIMENT

In this work, Pt/MgO/Pt MIM diodes were fabricated. The MgO films of 60 nm were deposited on Pt/Ti/SiO_2/Si substrates using *rf* magnetron sputtering in Ar ambient at room temperature. The MgO target was used. The *rf* power density was 1.1 W/cm^2. The flow rate of argon was 13.5 sccm. The pressure during deposition was 50 mTorr. A thermal treatment by rapid thermal annealing was performed at 400 °C for 60 s in nitrogen ambient. To achieve the MIM structure, a Pt top electrode was deposited by *dc* magnetron sputtering with a round area of 3.14×10^{-4} cm^2 patterned by the shadow mask process. The thickness of Pt top electrodes is 100 nm. The current-voltage (*I-V*) characteristics of the fabricated MgO-based RRAM devices were measured by Agilent 4156 C semiconductor parameter analyzer. During the measurement in voltage sweeping mode, the bias voltage was applied on the top electrode with the bottom electrode grounded. All the measurements were performed under dark condition.

III. RESULTS AND DISCUSSION

A typical current density-electric field (*J-E*) switching characteristic in the Pt/MgO/Pt structure is shown in Fig. 1. The symmetric *J-E* curves are found in the Pt/MgO/Pt structure. In this work, when a sweep voltage is applied from 0 to +10 or −10 V with a current compliance of 1 mA, an abrupt increase of the device current takes place at a threshold voltage. The threshold voltage triggers the memory cell from a HRS to a LRS, which is defined as the "SET" process.

[a)]Author to whom correspondence should be addressed. Electronic mail: FCChiu@mail.mcu.edu.tw.

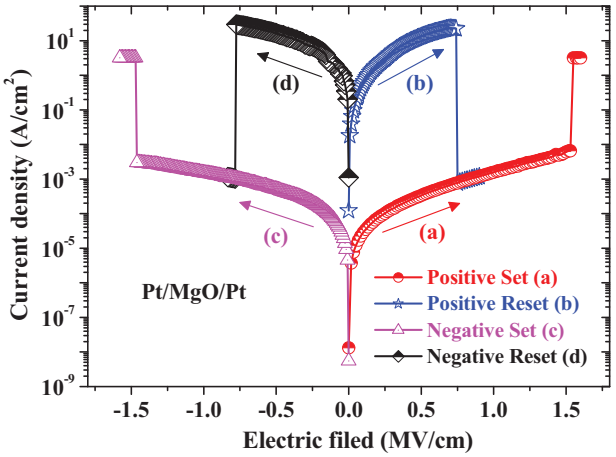

FIG. 1. Typical nonpolar *J-E* switching characteristics of Pt/MgO/Pt memory cells.

Hence, the threshold voltage is named as set voltage (V_{set}). On the other hand, by re-sweeping the voltage in positive or negative side without a current compliance, the device current decreases suddenly at a reset voltage (V_{reset}) and the device is switched from LRS to HRS. In this event, it is defined as the "RESET" process. The RESET into the HRS takes place at a higher current and a voltage smaller than the SET voltage. Based on the *J-E* switching characteristic in Fig. 1, the MgO RRAM device may be electroforming-free or the electroforming process is accompanied with the first SET process by considering the SET voltages at the range of 10 V. This result may come from the relatively high density of defects produced in the MgO films during the process of *rf* magnetron sputtering. This clear reversible and reproducible switching between LRS and HRS is observed at temperatures ranging from 300 to 450 K. Figure 2 shows that the SET and RESET fields are around 1.5 MV/cm and 0.7 MV/cm, respectively. Both the SET and RESET processes are independent of voltage polarity in this work. Hence, the RS in Pt/MgO/Pt structure is nonpolar. The nonpolar RS shows the coexistence of unipolar and bipolar RS characteristics. Reports show that the nonpolar switching characteristic is also observed in the RRAM memory devices using the dielectrics of TiO_2,[16] NiO,[17] CoO,[17] Fe_2O_3,[17] V-doped $SrZrO_3$,[5] Cu-doped SiO_2,[18] and Cu-doped ZrO_2.[19,20]

During the dc voltage sweep measurements for the SET process, the current is required to be limited by a compliance current (I_{comp}) for protecting the RRAM devices from the permanent damage. Figure 2 shows the dependence of I_{comp} on LRS resistances (R_{LRS}) after the SET processes in different Pt/MgO/Pt memory devices. The cumulative probability distribution of R_{LRS} as a function of I_{comp} is made by the Weibull plot, as shown in the inset of Fig. 2. When the I_{comp} is not less than 0.5 mA, the R_{LRS} values are approximately centered on the order of 10^2–10^3 Ω and show slight variations. The same phenomenon was also observed in the CoFeB/MgO/CoFeB structure.[12] Report indicates that the reset current (I_{RESET}) increases as the filament diameter increases.[21] This implies that using enough I_{comp} ($\geq$0.5 mA) during SET process, a maximum size of built filamentary channels in MgO films seems to be approached in this work. Therefore, the approximately constant R_{LRS} is obtained. On the other hand, for I_{comp} smaller than 0.5 mA during SET process, the built filamentary channels are incomplete, which makes the LRS resistances large and variational. Figure 3 shows the dependence of I_{comp} on I_{RESET}. The cumulative probability distribution of I_{RESET} is shown in the inset of Fig. 3. The I_{RESET} values are approximately centered on the order of 10^{-4}–10^{-3} A when $I_{comp} \geq 0.5$ mA. This suggests that the rupture of the uniformly built filamentary channels can be done by the satisfied I_{RESET}. According to Figs. 2 and 3, R_{LRS} and I_{RESET} are approximately independent of I_{comp} as $I_{comp} \geq 0.5$ mA because the sizes of built filamentary channels are about the same in MgO thin films. This result is a new finding for RRAM devices. It is worthy to note that a serious I_{comp} overshoot problem may be observed during SET process in 1 R-architecture $TaN/Cu_xO/Cu$ RRAM device in the case of small I_{comp}.[22] Wan *et al.* indicated that R_{LRS} has a negative relationship with I_{comp} when $I_{comp} \geq 1$ mA. However, when I_{comp} is below 1 mA, R_{LRS} is independent of I_{comp} because of the effect of parasitic

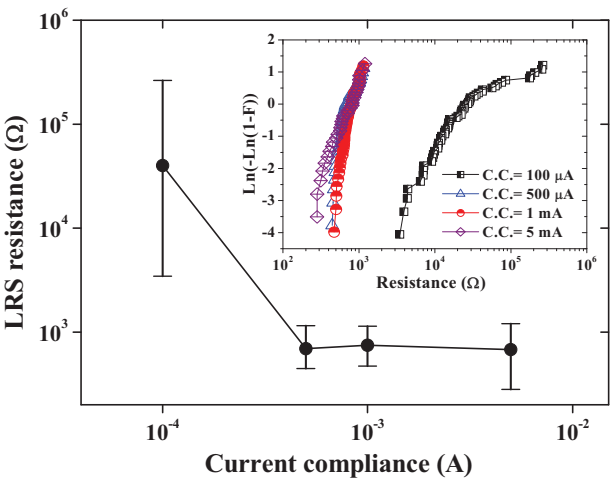

FIG. 2. Dependence of current compliance on LRS resistances (R_{LRS}) after the SET processes. Inset graph shows the cumulative probability distributions of R_{LRS} as a function of I_{comp}.

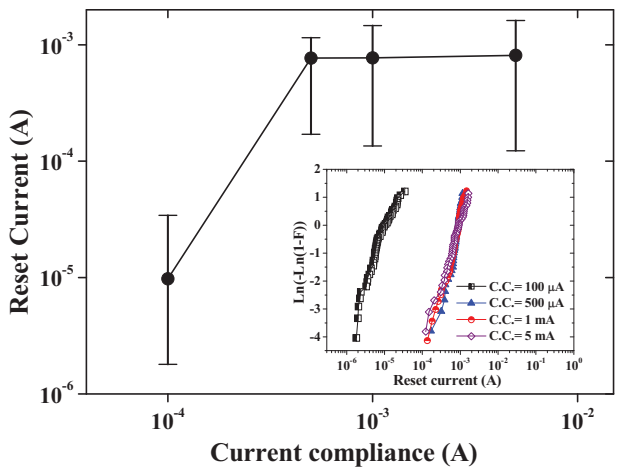

FIG. 3. Dependence of current compliance on RESET current (I_{RESET}). Inset graph shows the cumulative probability distributions of I_{RESET} as a function of I_{comp}.

capacitance in 1 R architecture. Owing to the excellent control of I_{comp} with the aid of gate voltage of the transistor, the I_{comp} overshoot problem can be solved by using 1T1R architecture. In this work, R_{LRS} is independent of I_{comp} when $I_{comp} \geq 0.5$ mA in Pt/MgO/Pt devices. This phenomenon should not come from the I_{comp} overshoot problem but the saturated filament size. The same conclusion is also suitable for the I_{RESET} in Pt/MgO/Pt devices.

Since various conduction mechanisms[23] depend on temperature in different ways, measuring the conduction current as a function of temperature will provide very useful information on the constitution of the conduction currents. In this work, the conduction mechanisms of Schottky emission, Poole-Frenkel emission, Fowler-Nordheim tunneling, direct tunneling, space-charge-limited conduction, Ohmic conduction as well as hopping conduction were studied for the Pt/MgO/Pt structure.[23] In general, the dominant conduction mechanism can be deduced from the typical plots of the *J-E* characteristics for each conduction mechanism. Hence, the temperature dependence of *J-E* characteristics both in HRS and LRS were measured to identify the current conduction mechanism in the Pt/MgO/Pt structure. Figure 4 shows the *J-E* characteristics at temperatures ranging from 300 K to 425 K under the condition of 1 mA compliance current. An interesting observation is found, i.e., a lower current density is obtained in a higher temperature. This finding is far different from the normal *J-E* characteristics of dielectrics in which the higher current density is obtained in a higher temperature. To investigate the physical mechanism, a simulation work was adopted. The simulation results show that experimental data match the theory of hopping conduction very well when the electric field is larger than about 0.25 MV/cm, as shown in Fig. 4. In hopping conduction, the carrier energy is lower than the maximum energy of the potential barrier between two trapping sites, as depicted in the inset of Fig. 5. Thus, the carrier transportation in MgO is with the aid of tunneling effect in HRS. The hopping conduction can be expressed as[23]

$$J = qanv \exp\left[\frac{qaE}{kT} - \frac{\Phi_t}{kT}\right], \quad (1)$$

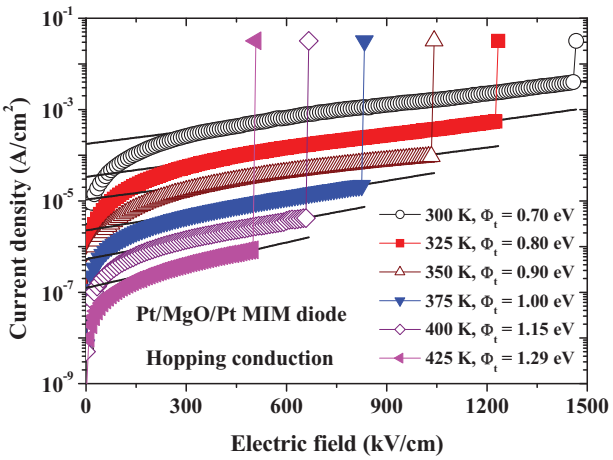

FIG. 4. Experimental data and simulation curves of hopping conduction in HRS in Pt/MgO/Pt memory cells.

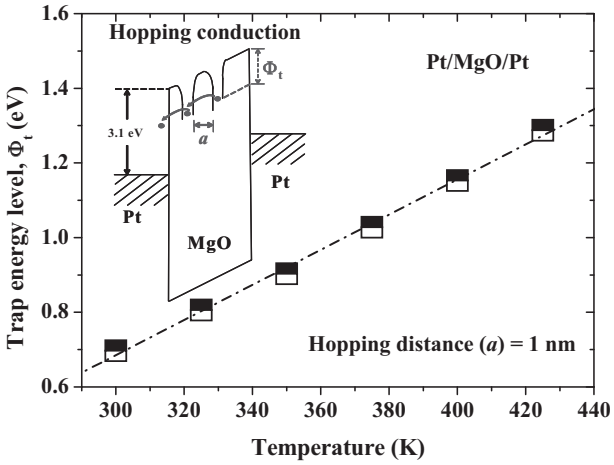

FIG. 5. Temperature dependence of the trap energy levels in HRS. Inset graph shows the band diagram of hopping conduction in Pt/MgO/Pt memory cells.

where q is the electronic charge, a is the mean spacing between trap sites (i.e., the hopping distance), n is the electron concentration in the conduction band of the dielectric, v is the frequency of thermal vibration of electrons at trap sites, E is the applied electric field, T is the absolute temperature, k is Boltzmann's constant, and Φ_t is the energy level from the trap states to the bottom of conduction band (E_C). According to Eq. (1), the trap spacing can be extracted by the slope of linear part of $\log(J)$ versus E. Therefore, the trap spacing in MgO is determined to be about 1.0 nm from Fig. 4. In addition, the temperature dependence of the trap energy levels in MgO is obtained, as shown in Fig. 5. The trap energy levels increase with increasing temperature. This result indicates that the defects with deeper level are activated by the elevated temperature. Hence, the deeper trap level activated at higher temperature leads to the exponential decrease in current density. These trap levels in MgO films determined in this work may come from the F centers which are the deep electron traps.[24] At 300 K, the trap level is about 0.7 eV. It is noted that no dominant conduction mechanism is found for the electric field smaller than about 0.25 MV/cm. Report showed that the conduction band offset (ΔE_C) between MgO and Si is 1.5 eV.[6] In addition, the electron affinity of Si and the workfunction of Pt is 4.05[25]and 5.65 eV,[26] respectively. Accordingly, the ΔE_C between MgO and Pt is 3.1 eV which is a considerably high barrier for carrier transport through the electrode-dielectric interface. This implies that the dominant conduction mechanism should not be the electrode-limited conduction mechanism but the bulk-limited conduction mechanism. The bulk-limited conduction mechanism depends only on the properties of the dielectric itself. In this work, the dominant conduction mechanism in HRS is the hopping conduction which belongs to the bulk-limited conduction mechanism. Based on the electrical analyses in HRS, the band diagram of carrier transportation in hopping conduction is shown in the inset of Fig. 5.

In LRS, the current density increases with increasing temperature. The *J-E* curves are shown in Fig. 6 in a double-logarithmic plot. Combined with the data in HRS, the HRS/LRS resistance ratio is about on the order of 10^5 at 300 K

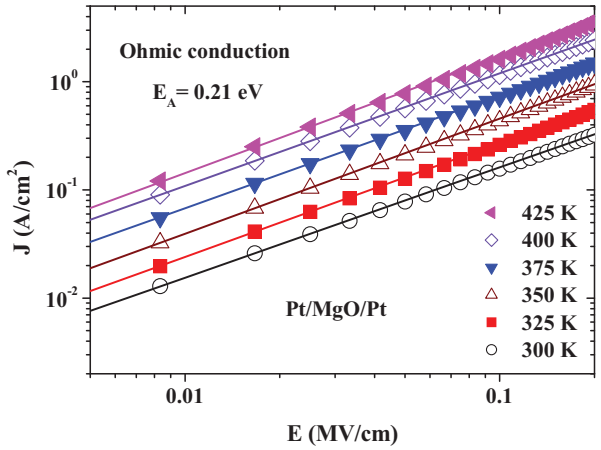

FIG. 6. Experimental data and simulation curves of Ohmic conduction in LRS in Pt/MgO/Pt memory cells.

and increases with increasing temperature in the Pt/MgO/Pt structure. Figure 6 shows the linear relationship between current density and electric field, which matches the Ohmic conduction very well in a low electric field (<0.2 MV/cm) because the slopes are very close to 1. The Ohmic conduction can be expressed as[23]

$$J = \sigma E = q\mu N_C E \exp\left[\frac{-(E_C - E_F)}{kT}\right], \qquad (2)$$

where σ is the electrical conductivity, μ is the electron mobility, N_C is the effective density of states of the conduction band, and E_F is the Fermi energy level; the other terms are as defined above. Fig. 7 shows the linear relationship between electrical conductivity and inverse temperature in LRS. According to the Arrhenius plot, E_F in LRS is determined to be about 0.21 eV below E_C, as shown in the inset of Fig. 7. Accordingly, the product of μ and N_C at each temperature can be extracted by the combination of E_F and σ. In addition, N_C is a function of temperature, which is proportional to $\beta T^{3/2}$, where β is a constant.[25] The electron mobility (μ) in MgO at room temperature is 20 cm^2/V s.[27] Therefore, the temperature

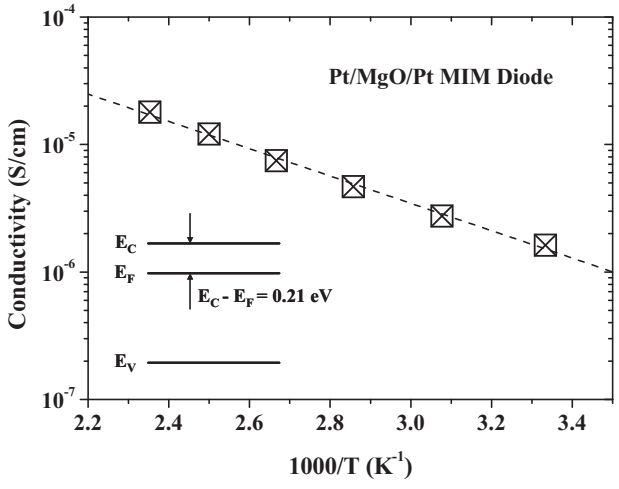

FIG. 7. Temperature dependence of the electrical conductivity in LRS. The inset graph shows the location of Fermi level in Ohmic conduction.

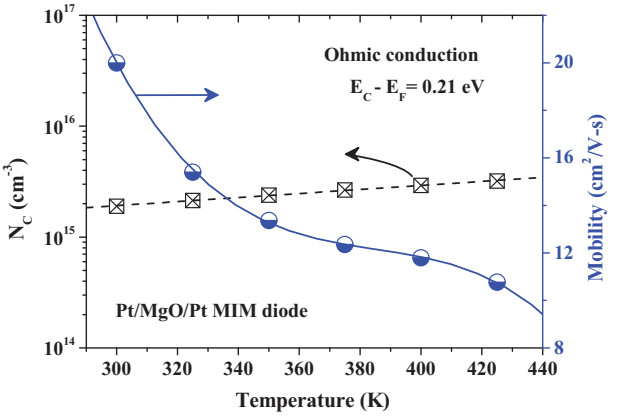

FIG. 8. Temperature dependence of the electron mobility and the effective density of states of the conduction band in LRS.

TABLE I. Electrical parameters of the nonpolar RS behavior in MgO films for the compliance current of 1 mA at 300 K.

Electrical parameter	Value
Mean SET field, E_{on} (MV/cm)	±1.5
Mean LRS[a] resistance, R_{on} (Ω)	~10^3
Mean RESET field, E_{off} (MV/cm)	±0.7
Mean HRS[b] resistance, R_{off} (Ω)	~10^8
HRS/LRS resistance ratio	~10^5
Spacing between trap sites (nm)	1.0
Trap energy level, E_C[c] $- E_t$ (eV)	0.70
Conduction band offset between Pt and MgO, ΔE_C (eV)	3.1
Fermi level in LRS in thermal equilibrium, $E_C - E_F$ (eV)	0.21
Electronic mobility in LRS, μ (cm^2/V s)	20
Effective density of states in conduction band in LRS, N_C (cm^{-3})	1.9×10^{15}

[a]Low resistance state.
[b]High resistance state.
[c]Bottom of conduction band.

dependence of μ and N_C in MgO can be obtained, as shown in Fig. 8. At 300 K N_C is about 1.9×10^{15} cm^{-3}. Table I lists the electrical parameters of the nonpolar RS behavior in MgO films for the compliance current of 1 mA at 300 K. In this work, experimental results indicate that the dominant conduction mechanism in MgO films is the hopping conduction during SET process. The hopping conduction is associated with the carrier tunneling among traps in the dielectric bulk. In addition, the sudden current increase in SET process is due to the formation of the conductive filaments in dielectric bulk.[2,6,22] Therefore, the switching mechanism of MgO RRAM devices is associated with trap-related conductive filaments.

IV. CONCLUSIONS

For the applications of next generation NVM devices, RRAM cells are studied to overcome the physical limitations of traditional Flash memory devices. The electrical properties of RRAM devices using MgO thin films were investigated in this work. Nonpolar resistance switching behavior is found in the Pt/MgO/Pt structure. Under the condition of

$I_{comp} \geq 0.5$ mA in SET processes, the LRS resistances and the RESET currents will reach their minimum and maximum, respectively. The current transportation in MgO films is dominated by the hopping conduction and the Ohmic conduction in HRS and LRS, respectively. Accordingly, the trap spacing and the trap energy levels were obtained in HRS. In addition, the Fermi level as well as the temperature-dependent electron mobility and effective density of states in conduction band in MgO were also obtained.

ACKNOWLEDGMENTS

The authors would like to thank the National Science Council, Taiwan, Republic of China for supporting this work under Contract No. NSC 98-2221-E-130-027-MY2.

[1]W. W. Zhuang, W. Pan, B. D. Ulrich, J. J. Lee, L. Stecker, A. Burmaster, D. R. Evans, S. T. Hsu, M. Tajiri, A. Shimaoka, K. Inoue, T. Naka, N. Awaya, K. Sakjyarma, Y. Wang, S. Q. Liu, N. J. Wu, and A. Ignatiev, Tech. Dig. - Int. Electron Devices Meet. 2002, 193.
[2]H. Akinaga and H. Shima, Proc. IEEE **98**, 2237 (2010).
[3]A. Sawa, Mater. Today **11**, 28 (2008).
[4]R. Waser, R. Dittmann, G. Staikov, and K. Szot, Adv. Mater. **21**, 2632 (2009).
[5]C. C. Lin, C. Y. Lin, M. H. Lin, C. H. Lin, and T. Y. Tseng, IEEE Trans. Electron Devices **54**, 3146 (2007).
[6]D. Ielmini, F. Nardi, and C. Cagli, IEEE Trans. Electron Devices **58**, 3246 (2011).
[7]M. Colle, M. Buchel, and D. M. de Leeuw, Org. Electron. **7**, 305 (2006).
[8]R. Müller, C. Krebs, L. Goux, D. J. Wouters, J. Genoe, P. Heremans, S. Spiga, and M. Fanciulli, IEEE Electron Device Lett. **30**, 620 (2009).
[9]S. H. Jo, K. H. Kim, and W. Lu, Nano Lett. **9**, 496 (2009).
[10]I. G. Baek, M. S. Lee, S. Seo, M. J. Lee, D. H. Seo, D. S. Suh, J. C. Park, S. O. Park, H. S. Kim, I. K. Yoo, U. I. Chung, and J. T. Moon, Tech. Dig. - Int. Electron Devices Meet. 2004, 587.
[11]E. Miranda, J. Martin-Martinez, E. O'Connor, G. Hughes, P. Casey, K. Cherkaoui, S. Monaghan, R. Long, D. O'Connell, and P. K. Hurley, Microelectron. Reliab. **49**, 1052 (2009).
[12]C. Yoshida, M. Kurasawa, Y. M. Lee, M. Aoki, and Y. Sugiyama, Appl. Phys. Lett. **92**, 113508 (2008).
[13]P. Krzysteczko, G. Reiss, and A. Thomas, Appl. Phys. Lett. **95**, 112508 (2009).
[14]H. H. Huang, W. C. Shih, and C. H. Lai, Appl. Phys. Lett. **96**, 193505 (2010).
[15]J. M. Teixeira, J. Ventura, R. Fermento, J. P. Araujo, J. B. Sousa, P. Wisniowski, and P. P. Freitas, J. Phys. D **42**, 105407 (2009).
[16]D. S. Jeong, H. Schroeder, and R. Waser, Electrochem. Solid-State Lett. **10**, G51 (2007).
[17]I. H. Inoue, S. Yasuda, H. Akinaga, and H. Takagi, Phys. Rev. B **77**, 035105 (2008).
[18]C. Schindler, S. C. P. Thermadam, R. Waser, and M. N. Kozicki, IEEE Trans. Electron Devices **54**, 2762 (2007).
[19]W. Guan, S. Long, Q. Liu, M. Liu, and W. Wang, IEEE Trans. Electron Devices **29**, 434 (2008).
[20]W. Guan, M. Liu, S. Long, Q. Liu, and W. Wang, Appl. Phys. Lett. **93**, 223506 (2008).
[21]U. Russo, D. Ielmini, C. Cagli, A. L. Lacaita, S. Spiga, C. Wiemer, M. Perego, and M. Fanciulli, Tech. Dig. - Int. Electron Devices Meet. 2007, 775.
[22]H. J. Wan, P. Zhou, L. Ye, Y. Y. Lin, T. A. Tang, H. M. Wu, and M. H. Chi, IEEE Electron Device Lett. **31**, 246 (2010).
[23]J. Y. M. Lee, F. C. Chiu, and P. C. Juan, "The application of high-dielectric-constant and ferroelectric thin films in integrated circuit technology," in *Handbook of Nanoceramics and Their Based Nanodevices*, edited by T. Y. Tseng and H. S. Nalwa (American Scientific Publishers, Los Angeles, California, USA, 2009), Vol. **4**, p. 159.
[24]T. Konig, G. H. Simon, H. P. Rust, G. Pacchioni, M. Heyde, and H. J. Freund, J. Am. Chem. Soc. **131**, 17544 (2009).
[25]S. M. Sze, *Physics of Semiconductor Devices*, 2nd ed. (Wiley, New York, 1981), p. 403.
[26]H. B. Michaelson, J. Appl. Phys. **48**, 4729 (1977).
[27]J. M. Warman, M. P. deHaas, P. Pichat, T. P. M. Koster, E. A. van der Zouwen-Assink, A. Mackor, and R. Cooper, Radiat. Phys. Chem. **37**, 433 (1991).